# Evaluation of Distributed OFDR-Based Sensing Performance in Mixed Neutron/Gamma Radiation Environments

Serena Rizzolo, Aziz Boukenter, Emmanuel Marin, Thierry Robin, Marco Cannas, Adriana Morana, Jocelyn Périsse, Jean-Reynald Macé, Youcef Ouerdane, B. Nacir, et al.

# Evaluation of Distributed OFDR-Based Sensing Performance in Mixed Neutron/Gamma Radiation Environments

S. Rizzolo, *Student Member, IEEE*, A. Boukenter, E. Marin, T. Robin, M. Cannas, A. Morana, J. Périsse, J-R Macé, Y. Ouerdane, B. Nacir, P. Paillet, *Senior Member, IEEE*, C. Marcandella, M. Gaillardin, *Member, IEEE*, and S. Girard, *Senior Member, IEEE*

***Abstract*— We report the study of a radiation resistant single mode optical fiber doped with fluorine exposed to mixed neutron and $\gamma$-radiation up to $10^{17}$ n/cm$^2$ fluence and >2 MGy dose to evaluate its performances when used as the sensing element of a distributed Optical Frequency Domain Reflectometry (OFDR). The use of complementary spectroscopic techniques highlights some differences between the responses of solely $\gamma$-radiation (10 MGy) or mixed neutron and $\gamma$ ($10^{17}$ n/cm$^2$+ > 2 MGy) irradiated samples. Those differences are linked to the defect generation rather than to structural changes of the $a$-$SiO_2$ host matrix. We show that a modification of the refractive index of $\sim 10^{-5}$ is induced at the highest investigated neutron fluence. However, the feasibility of distributed temperature measurements along the irradiated fiber is demonstrated with an accuracy of 0.1 °C over a sensing length up to ~ 130 m with the tested OBR4600 interrogator. These results are very promising for the integration of OFDR sensors in mixed neutron and gamma radiation environments.**

***Index Terms*— Neutrons, optical fiber sensors, radiation, Rayleigh scattering.**

## I. Introduction

OPTICAL fiber sensors (OFS) are more and more considered for integration in harsh environments characterized by moderate to high levels (doses and fluences) of radiation. Most of the studies have been devoted to the radiation effects on the transmission of optical fibers, highlighting that the radiation induced attenuation (RIA) is the most influential mechanism altering the signal propagation [1]. Other phenomena, such as radiation induced emission (RIE) or radiation induced refractive index change (RIRIC) affect also the performances of optical fibers in some applications [1]. While the RIA reduces the sensing length that can be used, the RIRIC will induce errors on the measured parameters due to the local evolution of the refractive index.

With the development of distributed sensors based on Raman, Brillouin or Rayleigh scattering, new radiation effects have been considered in addition to RIA, RIE and RIRIC. For Brillouin sensing, a Radiation-induced Brillouin Frequency Shift (RI-BFS) was observed and causes an additional error in the estimation of temperature or strain values by the systems, amplitudes of RI-BFS being, like the RIA, dependent on various parameters such as the fiber composition [2]. Raman sensors have been shown to be sensitive to the $\Delta$RIA used to evaluate the temperature along the sensing fiber, which, if not corrected [3], is responsible of huge errors on temperature responses of single-ended systems. Recent results have shown that Rayleigh sensors are more robust against total ionizing dose (TID): the temperature and strain coefficients are not affected nor by permanent effects up to at least 10 MGy(SiO2) irradiation dose [4] either by steady-state irradiation up to, at least, 1 MGy(SiO2) [5]. Nevertheless, fiber packaging influences the OFDR sensor response: radiation changes the mechanical properties of the coating surrounding the fiber core/cladding and can lead to errors in strain or temperature distributed measurements. Irradiations up to 3 MGy, as well as thermal treatments up to the maximum operating temperature of this surrounding coating, have been shown to improve the performances of the sensors under harsh environments [6], [7].

In this work we investigate the behavior of OFDR sensors to fission neutrons (0.8 MeV) at fluences up to $10^{17}$ n/cm$^2$. The explored fluence levels are representative of several applications within nuclear power plants (NPPs) covering both their nominal or accidental operations. The feasibility of OFDR temperature measurements was already demonstrated in nuclear reactor [8], under a neutron flux of $1.2 \times 10^{13}$ n/cm$^2$s and $\gamma$-dose rate of 1 MGy/h. Previous studies performed at comparable fluences but with 14 MeV neutrons [9], demonstrate that X-rays, $\gamma$-rays and neutrons globally lead to the same defect generation mechanisms and the same class of defects contributes to the induced losses in fluorine-doped optical fiber i.e. E' center, ≡Si·, nonbridging oxygen

S. Rizzolo is with Univ. Lyon, Lab.Hubert Curien, CNRS UMR 5516, Saint-Etienne, France and also with Dipartimento di Fisica e Chimica, Universià di Palermo, Palermo 90133, Italy and also with Areva Centre Technique, Le Creusot 71200, France (e-mail: rizzoloserena@gmail.com).

A. Boukenter, E. Marin, A. Morana, Y. Ouerdane, and S. Girard are with Univ. Lyon, Lab.Hubert Curien, CNRS UMR 5516, Saint-Etienne, France.

T. Robin is with iXBlue, Lannion 22300, France.

M. Cannas is with Dipartimento di Fisica e Chimica, Universià di Palermo, Palermo 90133, Italy.

J. Périsse is with Areva NP, Lyon 69006, France.

J-R Macé is with Areva NP, Paris-La Défense 92084, France.

B. Nacir is with the Centre National de l'Energie, des Sciences et des Techniques Nucléaires, Maamoura, Morocco.

P. Paillet, C. Marcandella, and M. Gaillardin are with CEA, DAM DIF, Arpajon, 91297, France.

hole center (NBOHC), ≡Si−O·; peroxy radical (POR), ≡Si−O − O·; and H(I), O =Si· − H. However, neutrons may affect more strongly the acrylate or polyimide coating material than $\gamma$ -rays and, as already mentioned, coating alteration can impact the OFDR response by modifying the internal stress distribution in the fiber transverse cross section [6]. Moreover, previous studies reveal that, above $10^{17}$-$10^{18}$ n/cm$^2$, the silica amorphous structure is directly affected by displacement damage [10] that may act on the sensor performances exploiting the Rayleigh signature of the amorphous glass.

Consequently, the understanding of generation mechanisms of these defects is relevant to improve the radiation resistance of optical fibers. Previous studies have shown that pure silica core (PSC) and F-doped fibers exhibit lowest RIA levels in both UV-Visible [1] and infrared (IR) [4] spectral domains for high irradiation doses; they are, for this reason, of particular interest for the design of radiation hardened distributed fiber sensors for nuclear industry.

The purpose of this work is to study the response of fluorine doped single mode fiber as OFDR-based sensor in mixed $\gamma$ and neutron environments. This radiation hardened optical fiber shows good OFDR sensing properties at MGy dose levels and for irradiation temperature range of [30 °C– 100 °C] [5].

The evaluation at the system level is combined to a spectroscopic analysis (absorption, confocal micro-luminescence and electron paramagnetic resonance - EPR) on the point defects generated under mixed neutrons/gamma and pure gamma environments allowing a better comprehension on the involved mechanisms at the basis of the radiation induced effects.

## II. Experimental Details

We tested a fluorine (F)-doped single mode fiber (SMF) developed by iXBlue manufacturer with an acrylate coating (maximum operating temperature 80°C). The sizes of core and cladding diameters are $\sim 10$ $\mu$m and $\sim 125$ $\mu$m, respectively, and the fluorine concentration is about 0.2 wt.% in the core and $\sim 1.5$ wt.% in the cladding. We investigated the properties of non-irradiated fiber as well as those exposed to a mixed neutron and $\gamma$ -ray environment up to neutron fluences of $10^{17}$ n/cm$^2$ and $\gamma$ -doses $>2$ MGy.

The neutron irradiations were performed at:

- The PROSPERO reactor of the Commissariat à l'énergie atomique et aux énergies alternatives (CEA), (Valduc, France) to reach fluences between $10^{13}$ n/cm$^2$ and $10^{14}$ n/cm$^2$ of fission neutrons (0.8 MeV) (with an additional $\gamma$ -dose in the kGy level).
- The 2 MW pool-type TRIGA Mark II reactor of the CNESTEN, Centre National de l'Energie, des Sciences et des Techniques Nucléaires, (Maamoura, Morocco). The accumulated fluence of fast neutrons (>9 keV) varies between $10^{15}$ n/cm$^2$ (with an additional $\gamma$ -dose of 0.02 MGy) and $10^{17}$ n/cm$^2$ (with an additional $\gamma$ -dose higher than 2 MGy).

Distributed temperature and strain measurements were carried out after irradiation (*post-mortem*) with an OBR 4600 from Luna Technologies equipped with a laser probe source centered at 1550 nm (accuracy of 1.5 pm) and tuned over a range of 21 nm. The spatial resolution was 40 $\mu$m for the scattering pattern along a maximum fiber length of 70 m, and was set to 1 cm and 0.2 cm for distributed temperature and strain measurements, respectively.

According to our previous studies [6], [7], we performed a pre-thermal treatment up to the maximum operating temperature of the acrylate coating, i.e. the maximal temperature it can resist without degrading the fiber properties, to stabilize the fiber/coating configuration and consequently the fiber temperature coefficient $C_T$ values. The temperature profile of the thermal treatment was set from 30 °C to 80 °C with an incremental step $\Delta$T of 5°C. The fibers were maintained at the same temperature for each step for half an hour.

Temperature calibration was done in stabilized oven controlled with a type K thermocouple; each fiber temperature sensitivity coefficient, $C_T$, was determined from the linear slope response of the Rayleigh spectral shift with temperature. For such experiments, all the samples, both non-irradiated and irradiated ones, were spliced to each other in series to perform the temperature treatment at the same time on a sample segment of $\sim 12$ m long.

Strain was induced by stretching the samples with a translation set up coupled to an adapted tensile gauge for both the evaluation of the applied constraint and its stability during the measurement. The strain applied along the fiber is given by the relation: $\varepsilon = \Delta L/L$, where L ($\Delta$L) is the length (extension) of the stretched fiber ($\sim 50$ cm). Strain sensitivity coefficient, $C_\varepsilon$, was determined from the slope of the Rayleigh spectral shift with strain in the range [$\sim 0$ $\mu\varepsilon - 4000$ $\mu\varepsilon$].

RIA in the visible spectral range was measured with the cutback method; we injected light from a Halogen source into the sample; the signal transmitted through the fiber link was analyzed with a UV-Visible optimized spectrometer from 200 to 900 nm. The infrared contribution was evaluated at 1550 nm with an Optical Time Domain Reflectometer (OTDR, EXFOFTB-7400E) [11]. The measurements were performed with a signal pulse width of 10 ns and an exposure time of 180 s.

Confocal micro-luminescence and micro-Raman (CML-R) measurements were performed to investigate the distributions of neutron and gamma induced active optical centers and profiles along the fiber transverse cross sections by using an Aramis spectrometer associated with a He-Cd ion laser excitation line (energy 325 nm (3.8 eV)) and supplied with a CCD camera, micro translation stages and a $\times 40$ objective. The employed experimental conditions lead to a spatial resolution of about $3\mu$m.

The EPR was used to identify and quantify the paramagnetic centers induced by the radiation. E'-Si and H(I) defects are probed at room temperature (300 K), whereas NBOH and POR centers were checked at low temperature (77K) using a Bruker EMX-Micro Bay spectrometer working at 9.8 GHz with a magnetic-field modulation frequency of 100 kHz. The absolute concentration of defects was estimated by comparing the double integral of the EPR spectrum with a reference silica sample. To this aim, we used an irradiated silica bulk sample whose E' concentration was known by spin-echo measurements, the accuracy of the absolute concentration

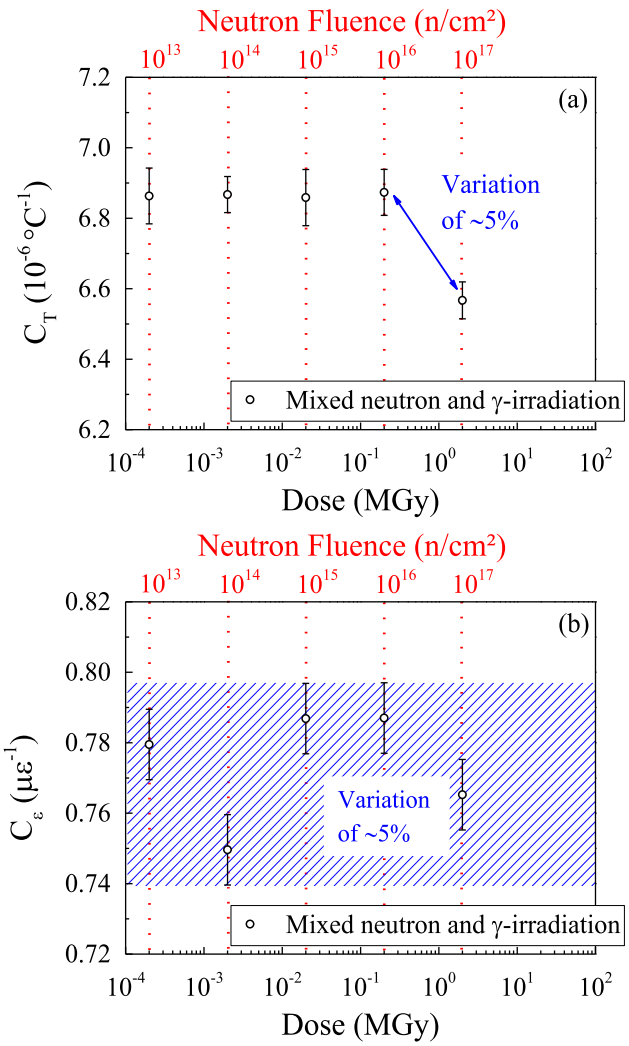


Fig. 1. (a) Temperature and (b) strain coefficients as a function of the total deposited dose (expressed in MGy [13]) for mixed neutron and $\gamma$-irradiated fibers. The associated neutron fluence is reported in the top horizontal-axis.

being estimated as 50% whereas the relative error among the different defect types is about 20% [12].

In order to understand the effect of the mixed radiation environment on OFDR-based sensors we studied the trend of temperature and strain coefficients as a function of the total deposited neutron fluence and gamma dose. To highlight a direct comparison with $\gamma$-rays, from the total accumulated fluence (expressed in n/cm$^2$) we calculate the equivalent deposited dose (in MGy) using the converting factor 1 Gy(SiO$_2$) equal to $2 \times 10^{12}$ n/cm$^2$ to sum up the additional $\gamma$-dose [13].

## III. Experimental Results

### A. Distributed Sensing

In this section we report the results on OFDR distributed sensors to investigate their response to mixed exposure. The comparison with only-$\gamma$ irradiated samples, investigated in [14], will be discussed later.

The results of $C_T$ and $C_\varepsilon$ as a function of the equivalent total dose are reported in Fig. 1 (a) and Fig. 1 (b). In the case of $C_T$, we note that mixed radiation affects $C_T$s only for the highest

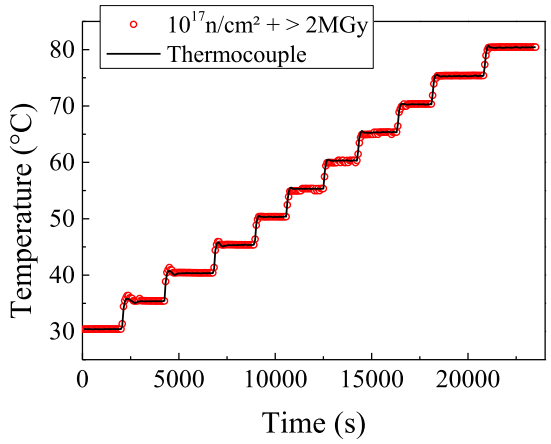


Fig. 2. Temperature evolution as a function of the time measured on the ($10^{17}$ n/cm$^2$+ > 2 MGy) sample (open red circles) and compared with thermocouple reference results (black line).

dose (i.e. $10^{17}$ n/cm$^2$+ > 2 MGy) where the coefficient varies of 5 % with respect to the others values. This variation, if not taken into account in temperature measurements, allows an error on distributed measurement due to the temperature calibration up to $\sim$ 3 °C at 80 °C. In the case of C$\varepsilon$s, the dose dependence is not as precisely determined due to the complexity of the measurements: we find that the values are indeed scattered within a variation of 5%, highlighted by the blue rectangle in Fig. 1 (b).

Once the $C_T$ is determined, the performances of temperature OFDR-sensors have been tested. The measurement as a function of the time is reported in Fig. 2 for the entire temperature profile. We can note that temperature, measured with the sample irradiated at the highest dose, is well determined during the experiment. The comparison with thermocouple results allows estimating the accuracy of our measurement: we obtain pretty good performances, being the temperature well determined with a precision of 0.1 °C in each step from 30 °C to 80 °C.

### B. Spectroscopic Analysis

In this section we report the results obtained by coupling diverse spectroscopic techniques. The investigation was performed on both mixed and only-$\gamma$ irradiated samples and the results are directly compared for each technique.

Fig. 3 (a) and Fig. 3 (b) display RIA in the visible spectrum and at 1550 nm as a function of the equivalent deposited dose, respectively. The measure of the RIA in the visible is compared for the two samples irradiated at higher doses (i.e. $10^{17}$ n/cm$^2$+ > 2 MGy and 10 MGy). Our results highlight at least two different contributions to the attenuation. We find an UV-absorption tail which increases at shorter wavelengths and an absorption band centered at around 630 nm that is well associated with the NBOHC defects [15].

We can observe that RIA level is higher in the mixed neutron and $\gamma$ irradiated sample than in the only-$\gamma$ irradiated one with RIA levels of $\sim$ 6 dB/m and $\sim$ 3 dB/m respectively. In the IR, we observe that, for mixed neutron and $\gamma$-irradiated

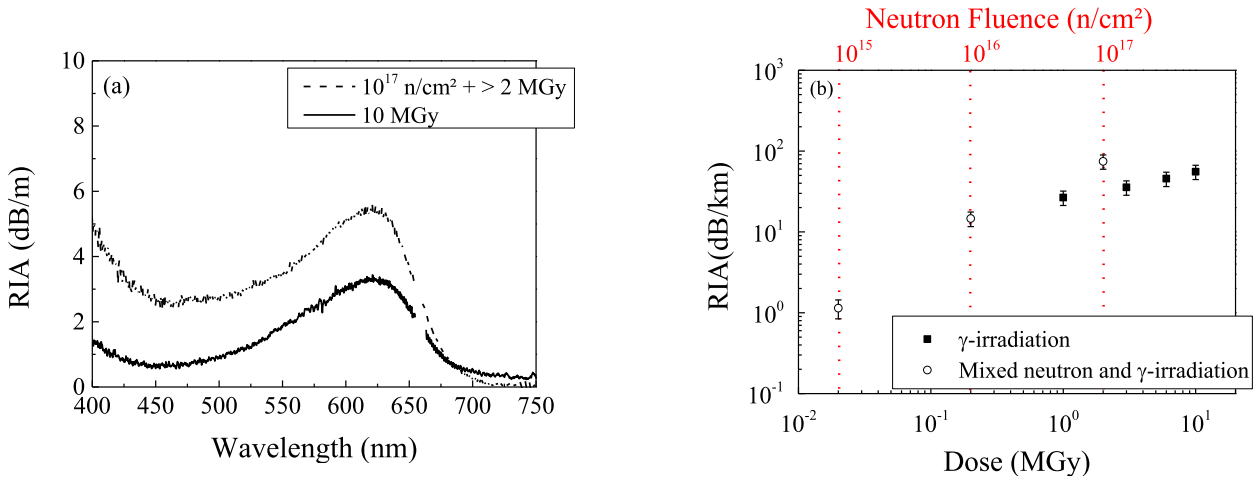


Fig. 3. (a) RIA spectra in UV-Visible range for mixed neutron fluence and $\gamma$-rays at $10^{17}$ n/cm$^2$+ > 2 MGy (black dotted line) and with only $\gamma$-rays at 10 MGy (black solid line). (b) Radiation induced attenuation of studied optical fibers at 1550 nm as a function of the total deposited dose (expressed in MGy [13]) for mixed neutron and $\gamma$-irradiated fiber (open circles) and only ã-irradiated fiber (solid squares adapted from [4]).

samples, RIA at 1550 nm starts to increase with radiation at $10^{15}$ n/cm$^2$ and reaches 75 dB/km at the highest fluence, whereas for lower fluences ($10^{13}$ and $10^{14}$ n/cm$^2$) RIA remains negligible in our samples being the attenuation similar to non-irradiated sample ($\sim$ 0.4 dB/km). From the comparison with $\gamma$-irradiated samples (data are adapted from [4]), we note that at the highest fluence RIA is higher than after a 10 MGy $\gamma$-dose irradiation (55 dB/km) remaining within the same order of magnitude.

Thanks to the CML technique it was possible to investigate the photoluminescence (PL) properties of pre-existing and induced defects to highlight the differences in their generation during mixed or only gamma exposures. Fig. 4 reports the comparison between not-irradiated and irradiated samples with the highest doses: $10^{17}$ n/cm$^2$+ > 2 MGy and 10 MGy. PL spectra in both core and cladding zones (Fig. 4 (a) and Fig. 4 (b) respectively) show a band peaked around 650 nm, associated with the NBOHCs [16], [17] for which their radial distribution is reported in Fig. 4 (c) demonstrating the impact of the F-co-doping on their concentration [17]. These defects are mainly located in the fiber core, whereas in the cladding their concentration decreases towards the outside part of the fiber. It is worth noting that the concentration of NBOHC in the cladding decreases before in mixed neutron and $\gamma$ irradiated samples than in only-$\gamma$ irradiated ones, result better highlighted from the 2D maps in the whole fibers of Fig. 4 (e) and Fig. 4 (f), where we can note a higher luminescence signal of these centers in the cladding for the 10 MGy irradiated sample. Another PL band is observed in the green region with characteristics depending on the radiation nature: we find that it is peaked at 527 nm for $10^{17}$ n/cm$^2$+ > 2 MGy irradiated sample, whereas it is centered at 515 nm for 10 MGy irradiated sample. We acknowledge that a similar band was observed in [18], [19]; these finding suggest that neutrons induce an intrinsic peculiar defect characterized by this green photoluminescence. The radial distribution of the PL band at 530 nm, reported in Fig. 4 (d), reveals a difference between the two radiation sources. We find, indeed, that in mixed neutron and $\gamma$ irradiated sample the luminescence is one order of magnitude higher than in only $\gamma$-irradiated one and we note that the concentration increases in the core in mixed neutron and $\gamma$ irradiated sample, whereas it slightly decreases in $\gamma$ irradiated ones.

Fig. 5 reports EPR spectra in the 10 MGy irradiated sample: in Fig. 5 (a) one of the most common intrinsic defects, the E', characterized by axial symmetry; its EPR spectrum was recorded at RT. A variant of the E' center can be also observed in EPR spectra, the H(I) defect, reported in Fig. 5 (b), consisting of a dangling Si bond with one neighboring O substituted by a H atom. The hyperfine interaction between the unpaired electron and the H nucleus, with spin of 1/2, originates the doublet of 74 G. Also its spectrum was measured at RT.

In contrast to these centers, the oxygen-related defect signals (NBOHC and POR) are large ($\sim$ 30 G) and they overlap, so they cannot be distinguished at RT; so measurements at low temperature, (77 K liquid nitrogen), are needed to separate the two spectra, shown in Fig. 5 (c), whose relative contributions can be estimated by a deconvolution procedure.

The defect concentrations as a function of the equivalent dose are reported in Fig. 6. All defect concentrations increase with the dose, both in mixed neutron and $\gamma$ irradiated sample and in only-$\gamma$ irradiated ones.

We observe that POR and H(I) concentration is higher in mixed neutron and $\gamma$ irradiated samples that in only-$\gamma$ irradiated one, whereas we reach similar value of concentration in the case of E' and NBOH centers. E' centers exhibit the highest concentration of $\sim 10^{17}$ cm$^{-3}$.

In Fig. 7 we report the Raman spectra recorded in the samples irradiated at the highest doses, i.e. $10^{17}$n/cm$^2$+ > 2MGy and 10 MGy. The comparison evidences that the spectra remain almost unchanged, thus suggesting that the explored fluence range is not high enough to observe structural modifications induced on the silica matrix. However, we

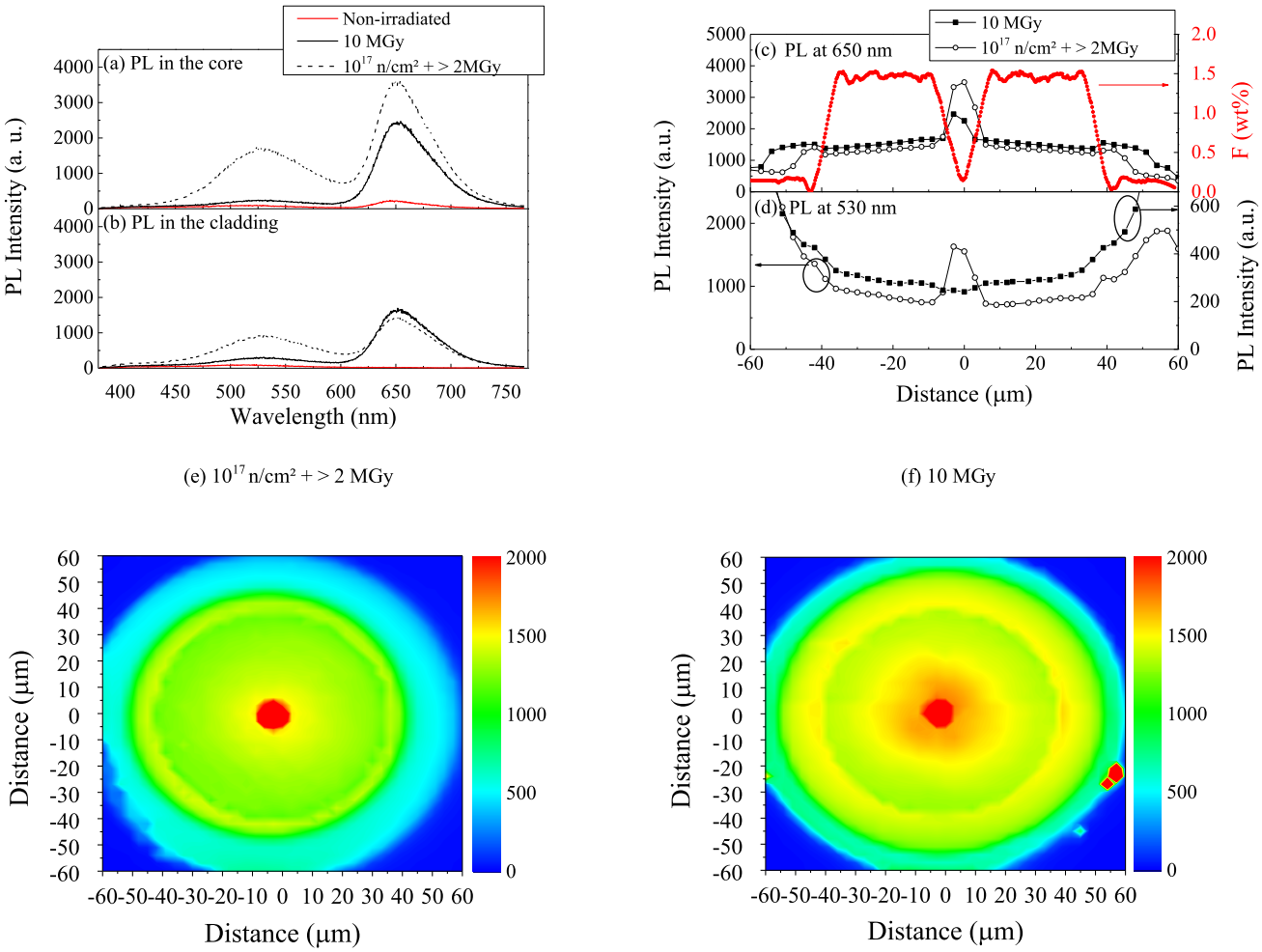


Fig. 4. PL spectra emitted from (a) the core center and (b) the cladding of the fiber irradiated with mixed neutron fluence and $\gamma$-rays at $10^{17}$ n/cm$^2$+ > 2 MGy (black dotted line) and with only $\gamma$-rays at 10 MGy (black solid line). (c) and (d) show PL intensity profiles along the diameter of 650 nm and 530 nm bands in $10^{17}$ n/cm$^2$+ > 2 MGy (open circles) and 10 MGy (solid squares) irradiated samples; red points represent the F-profile. In (e) and (f) the 2D maps of the emission at 650 nm are reported for mixed neutron fluence and $\gamma$-rays at $10^{17}$ n/cm$^2$+ > 2 MGy and only $\gamma$-rays at 10 MGy, respectively.

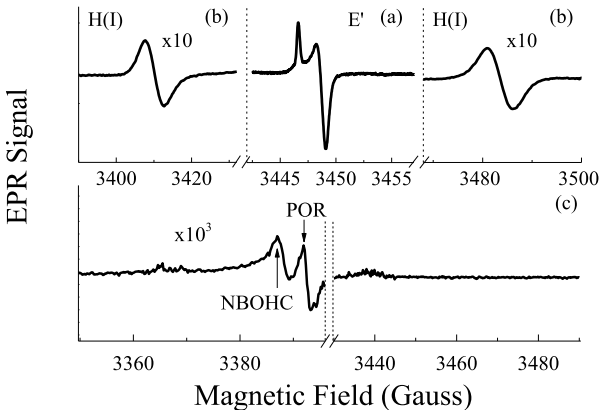


Fig. 5. EPR first harmonic spectra in the samples irradiated at 10 MGy. (a) shows E' center line, in (b) is shown the doublet of the H(I) center, and the (c) shows EPR spectrum associated with the NBOH and the POR centers.

observed slight differences on the bands at $\sim$ 800 cm$^{-1}$ and $\sim$ 1050 cm$^{-1}$ associated with the bending and the asymmetric stretching of Si-O-Si bridges [20].

## IV. Discussion

The investigation on distributed OFDR measurements in mixed neutron and $\gamma$ radiation environment reveal differences for the fluence of $10^{17}$ n/cm$^2$ and doses exceeding the MGy range. We have indeed observed a change in the $C_T$ of 5% at the highest dose. Comparing these results with those obtained in only $\gamma$-irradiated samples [14] we notice that the coefficient value corresponding to the highest fluences is similar to the 1 MGy irradiated sample (values are $(6.59\pm 0.02)\cdot 10^{-6}$ °C$^{-1}$ for the 1 MGy irradiated sample of reference [14] and $(6.58\pm 0.01)\cdot 10^{-6}$ °C$^{-1}$ in $10^{17}$ n/cm$^2$ irradiated sample) thus suggesting that both mixed neutron and $\gamma$-radiation at these fluences and doses can change the fiber response. As a first approximation, the radiation, by acting on the coating stabilization, changes the coating/fiber configuration according to the studies on thermic and mechanical properties on acrylate coated optical fibers of [21]. We have shown, however, that the $C_T$ change is not affecting temperature measurements that have shown good performances (accuracy of 0.1 °C) up to the highest temperature probed, i.e. 80°C.

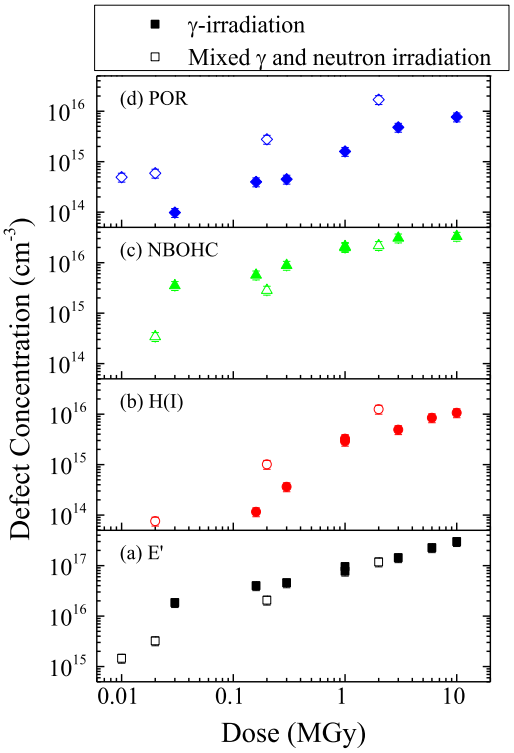


Fig. 6. Concentration of (a) Si- E', (b) H(I), (c) NBOHC and (d) POR point defects as a function total deposited dose [13]. Solid point indicated the only-$\gamma$ irradiated samples, whereas open point are mixed neutron and $\gamma$ irradiated ones.

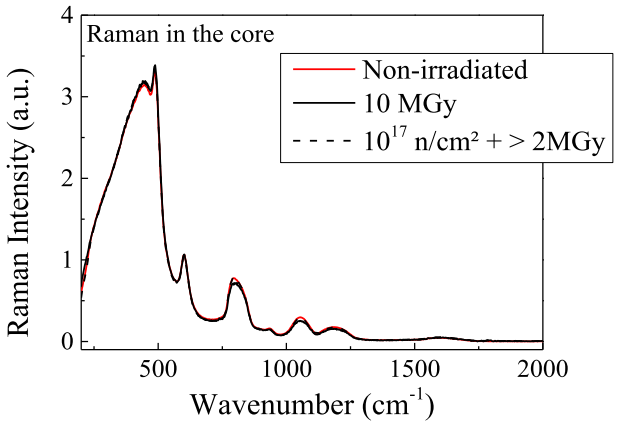


Fig. 7. Raman spectra recorded in the core center of $10^{17}$ n/cm$^2$+ > 2 MGy (black dotted line) and 10 MGy (black solid line) irradiated samples. The red line indicates the data obtained for non-irradiated sample.

To go further on the induced radiation effects, in Fig. 8 we have reported the spectral shift as a function of the fiber length path for different temperatures, acquired during the calibration.

We can observe that the spectral shift is pretty uniform along each sample, thus allowing a comparison of its value for the different doses. We note also that the value of recorded spectral shift is the same from non-irradiated sample to $10^{16}$ n/cm$^2$ + 0.2 MGy and that it changes for the highest doses. We have calculated this spectral shift difference (SSD)

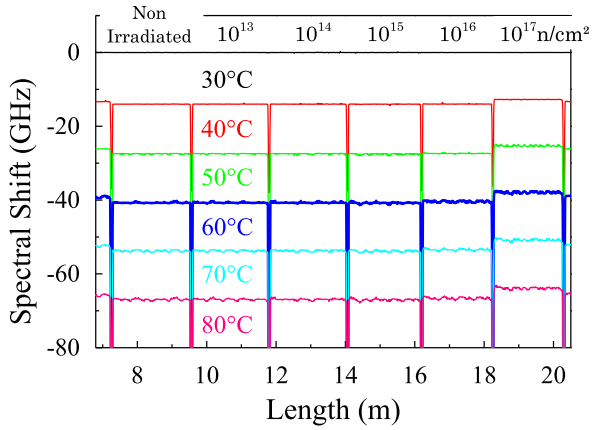


Fig. 8. Spectral shift as a function of the sample path length at some different temperature steps during the temperature calibration. The non-irradiated, as well as the irradiated segments are spliced to each other to perform the calibration in the same conditions for all the samples.

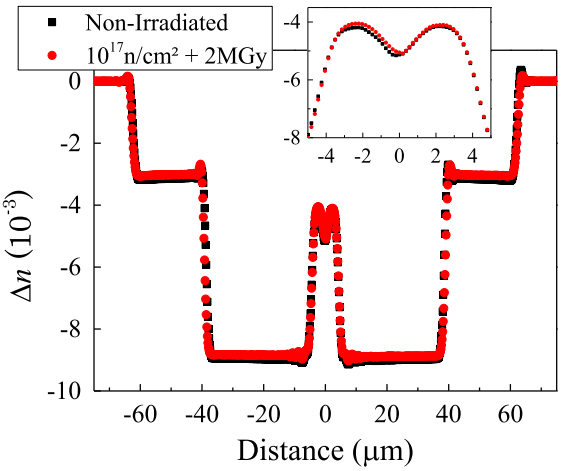


Fig. 9. Refractive index radial distributions in non-irradiated (black point) and $10^{17}$n/cm$^2$+ > 2MGy irradiated one (red points). The inset shows a zoom in the fiber core. The results are shown by taking the difference with respect the refractive index in the exterior part of the cladding.

between non-irradiated and $10^{17}$ n/cm$^2$+ > 2MGy obtaining that it is function of the temperature: 0.6 GHz for 40 °C up to 3.6 GHz at 80 °C.

It is well known that the Rayleigh signature of a given fiber is dependent on the refractive index fluctuation along its length [22], [23], fluctuation which also influences the spectral shift calculation by [24]:

$$-\frac{\Delta\nu}{\nu_C} = \frac{\Delta n}{n} \tag{1}$$

where $\nu_C = c/\lambda_C$, with $c$ the speed of the light and $\lambda_C = 1550$ nm, and $n$ the refractive index of the fiber core. Then, from the measured values of SSD we are able to estimate the refractive index variation in $10^{17}$ n/cm$^2$+ > 2MGy irradiated sample finding values from $\sim 0.5 \cdot 10^{-5}$ at 40 °C to $\sim 3 \cdot 10^{-5}$ at 80 °C. These values of refractive index variations induced by mixed exposure are in agreement with those obtained from $\Delta n$ radial measurements, reported in Fig. 9, from which we have extracted the variation of $n$with $\sim 7 \cdot 10^{-5}$ in the fiber core, see

inset of Fig. 8, (it is worth noting that obtained refractive index variation values are near the limit imposed by the experimental technique).

The use of complementary spectroscopic techniques has allowed studying the main radiation effects at the microscopic scale and estimating the differences induced by the two environments here considered. We have found that both mixed neutron and $\gamma$ and only- $\gamma$ irradiations lead to the generation of the same defects as highlighted from absorption, luminescence and EPR measurements. We have observed that the radiation induced losses are higher in $10^{17}$n/cm$^2$+ $>$ 2MGy than 10 MGy irradiated samples, even if they remain in the same order of magnitude. These findings agree with the study reported by Henschel et al., where it is shown that $\gamma$ and neutron irradiations lead to the same induced losses if the fluences is $<10^{14}$ n/cm$^2$ whereas higher fluences of neutrons cause higher losses than $\gamma$ irradiation [25].

## V. Conclusion

In this work we have reported the characterization of an F-doped single mode optical fiber exposed to mixed neutron and $\gamma$-radiation to evaluate its performances as sensing element of distributed an OFDR-sensors.

The use of complementary spectroscopic techniques has allowed studying the principal radiation effects such as RIA, photoluminescence and EPR of induced point defects. We have found that the main effect induced by both kinds of radiations is the generation of point defects such as E', NBOHC, H(I) and POR which generate similar absorption and EPR properties. Luminescence investigation has evidenced that the presence of neutrons affects differently the radial distribution of the NBOHC. Moreover, a green luminescence band, centered at $\sim$ 527 nm, is peculiarly observed in mixed neutron and $\gamma$-irradiated samples.

Furthermore, the calibration measurement of an OFDR-sensor has shown that a modification of the refractive index of $\sim$ $10^{-5}$ is induced by the exposure to mixed radiation environments. Nevertheless, the feasibility of distributed temperature measurements is demonstrated with an accuracy of 0.1 °C at the highest investigated doses of $10^{17}$ n/cm$^2$+ $>$ 2MGy, thus suggesting that the RIRIC acts on temperature coefficient, which became function of the refractive index:

$$C_T \rightarrow C_T(n) \quad (2)$$

Even if the sensing parameters dependence on refractive index has to be further investigated to improve and to predict their behavior radiation environments, reported results have shown that OFDR remains a promising solution for the development of distributed sensors also in mixed environments with presence of neutrons.

## References


[1] S. Girard *et al.*, "Radiation effects on silica-based optical fibers: Recent advances and future challenges," *IEEE Trans. Nucl. Sci.*, vol. 60, no. 3, pp. 2015–2036, Feb., 2013.

[2] X. Phèron *et al.*, "High $\gamma$-ray dose radiation effects on the performances of Brillouin scattering based optical fiber sensors," *Opt. Exp.*, vol. 20, no. 24, pp. 26978–26985, 2012.

[3] D. Di Francesca *et al.*, "Radiation hardened architecture of a single-ended raman-based distributed temperature sensor," in *Proc. IEEE Trans. Nucl. Space Radiat. Effects Conf.*, Portland, OR, USA, Jul. 2016.

[4] S. Rizzolo *et al.*, "Vulnerability of OFDR-based distributed sensors to high $\gamma$-ray doses," *Opt. Exp.*, vol. 23, no. 15, pp. 18997–19009, 2015.

[5] S. Rizzolo *et al.*, "Radiation hardened optical frequency domain reflectometry distributed temperature fiber-based sensors," *IEEE Trans. Nucl. Sci.*, vol. 62, no. 6, pp. 2988–2994, Dec. 2015.

[6] S. Rizzolo *et al.*, "Radiation characterization of optical frequency domain reflectometry fiber-based distributed sensors," *IEEE Trans. Nucl. Sci.*, vol. 63, no. 3, pp. 1688–1693, Feb. 2016.

[7] S. Rizzolo *et al.*, "Investigation of coating impact on OFDR optical remote fiber-based sensors performances for their integration in high temperature and radiation environments," *J. Lightw. Technol.*, vol. 34, no. 19, pp. 4460–4465, Oct. 1, 2016, doi: 10.1109/JLT.2016.2552459.

[8] A. K. Sang, M. E. Froggatt, D. K. Gifford, S. T. Kreger, and B. D. Dickerson, "One centimeter spatial resolution temperature measurements in a nuclear reactor using Rayleigh scatter in optical fiber," *IEEE Sensors J.*, vol. 8, no. 7, pp. 1375–1380, Jul. 2008.

[9] S. Girard, J. Baggio, and J. Bisutti, "14-MeV neutron, $\gamma$-ray, and pulsed X-ray radiation-induced effects on multimode silica-based optical fibers," *IEEE Trans. Nucl. Sci.*, vol. 53, no. 6, pp. 3750–3757, Dec. 2006.

[10] M. León *et al.*, "Neutron irradiation effects on the structural properties of KU1, KS-4V and I301 silica glasses," *IEEE Trans. Nucl. Sci.*, vol. 61, no. 4, pp. 1522–1530, Aug. 2014.

[11] H. Henschel, O. Kohn, and H. U. Schmidt, "Radiation induced loss measurements of optical fibres with optical time domain reflectometers (OTDR) at high and low dose rates," in *Proc. 1st Eur. Conf. Radiat. Effects Devices Syst.*, La Grande-Motte, France, 1991, pp. 380–382.

[12] S. Agnello, R. Boscaino, G. Buscarino, M. Cannas, and F. M. Gelardi, "Structural relaxation of E$'_\gamma$ centers in amorphous silica," *Phys. Rev. B*, vol. 66, p. 113201, Sep. 2002.

[13] A. A. Witteles, "Neutron radiation effects on MOSFETs: Theory and experiment," *IEEE Trans. Nucl. Sci*, vol. 15, no. 6, pp. 126–132, Nov. 1968.

[14] S. Rizzolo *et al.*, "Coating impact and radiation effects on optical frequency domain reflectometry fiber-based temperature sensors," *Proc. SPIE*, vol. 9634, p. 96346U, Sep. 2015.

[15] A. Morana *et al.*, "Origin of the visible absorption in radiation-resistant optical fibers," *Opt. Mater. Exp.*, vol. 3, no. 10, pp. 1769–1776, 2013.

[16] L. Skuja, "The origin of the intrinsic 1.9 eV luminescence band in glassy $SiO_2$," *J. Non-Cryst. Solids*, vol. 179, pp. 51–69, 1994.

[17] L. Vaccaro *et al.*, "Influence of fluorine on the fiber resistance studied through the non-bridging oxygen hole center related luminescence," *J. Appl. Phys.*, vol. 113, no. 19, p. 193107-5, 2013.

[18] A. Morana *et al.*, "Influence of neutron and gamma-ray irradiations on rad-hard optical fiber," *Opt. Mater. Exp.*, vol. 5, no. 4, pp. 898–911, 2015.

[19] P. Martìn, M. León, and A. Ibarra, "Photoluminescence in neutron irradiated fused silica," *Phys. Status Solidi C*, vol. C2, no. 1, pp. 624–628, 2005.

[20] G. S. Henderson, D. R. Neuville, B. Cochain, and L. Cormier, "The structure of $GeO_2SiO_2$ glasses and melts: A Raman spectroscopy study," *J. Non-Cryst. Solids*, vol. 355, pp. 468–474, 2009.

[21] Y. Nakajima *et al.*, "A study for estimating thermal strain and thermal stress in optical fiber coatings," *Furukawa Rev.*, vol. 34, pp. 8–12, 2008.

[22] B. J. Soller, D. K. Gifford, M. S. Wolfe, and M. E. Froggatt, "High resolution optical frequency domain reflectometry for characterization of components and assemblies," *Opt. Exp.*, vol. 13, no. 2, pp. 666–674, 2005.

[23] S. Kreger *et al.*, "High-resolution extended distance distributed fiber-optic sensing using Rayleigh backscatter," *Proc. SPIE*, vol. 6530, p. 65301R, Apr. 2007.

[24] S. Leparmentier, J. L. Auguste, G. Humbert, G. Pilorget, L. Lablonde, and S. Delepine-Lesoille, "Study of the hydrogen influence on the acoustic velocity of single-mode fibers by Rayleigh and Brillouin backscattering measurements," *Proc. SPIE*, vol. 9634, p. 963432, Sep. 2015.

[25] H. Henschel *et al.*, "Comparison between fast neutron and gamma irradiation of optical fibres," *IEEE Trans. Nucl. Sci*, vol. 45, no. 3, pp. 1543–1551, Jun. 1998.